JNS SPINE

LABORATORY INVESTIGATION

Safety of mapping the motor networks in the spinal cord using penetrating microelectrodes in Yucatan minipigs

***Soroush Mirkiani, MSc,[1,2] Carly L. O'Sullivan, BSc,[1,2] David A. Roszko, MSc,[2,3] Pouria Faridi, MSc,[1,2] David S. Hu, BSc,[2,4] Dirk G. Everaert, PhD,[2,4] Amirali Toossi, PhD,[1,2,4] Ryan Kang, BSc,[2] Tongzhou Fang, BSc,[2] Neil Tyreman, BSc,[2,4] Ashley N. Dalrymple, PhD,[1,2,5] Kevin Robinson, PT, DSc,[6] Richard R. E. Uwiera, DVM, PhD,[2,7] Hamid Shah, MD,[8] Richard Fox, MD,[2,9] Peter E. Konrad, MD, PhD,[10,11] and Vivian K. Mushahwar, PhD[1,2,4]**

[1]Neuroscience and Mental Health Institute, University of Alberta, Edmonton, Alberta, Canada; [2]Institute for Augmentative and Restorative Technologies and Health Innovations (iSMART), University of Alberta, Edmonton, Alberta, Canada; [3]Edward S. Rogers Sr. Department of Electrical and Computer Engineering, University of Toronto, Ontario, Canada; [4]Division of Physical Medicine and Rehabilitation, Department of Medicine, University of Alberta, Edmonton, Alberta, Canada; [5]Department of Mechanical Engineering, Carnegie Mellon University, Pittsburgh, Pennsylvania; [6]School of Physical Therapy, Belmont University, Nashville, Tennessee; [7]Department of Agricultural, Food and Nutritional Science, University of Alberta, Edmonton, Alberta, Canada; [8]Vanderbilt University Medical Center, Nashville, Tennessee; [9]Division of Neurosurgery, Department of Surgery, University of Alberta, Edmonton, Alberta, Canada; and [10]Department of Neurosurgery, West Virginia University, Morgantown, West Virginia; and [11]Integrative Neuroscience & Clinical Innovation, Rockefeller Neuroscience Institute, Morgantown, West Virginia

OBJECTIVE The goal of this study was to assess the safety of mapping spinal cord locomotor networks using penetrating stimulation microelectrodes in Yucatan minipigs (YMPs) as a clinically translational animal model.

METHODS Eleven YMPs were trained to walk up and down a straight line. Motion capture was performed, and electromyographic (EMG) activity of hindlimb muscles was recorded during overground walking. The YMPs underwent a laminectomy and durotomy to expose the lumbar spinal cord. Using an ultrasound-guided stereotaxic frame, microelectrodes were inserted into the spinal cord in 8 animals. Pial cuts were made to prevent tissue dimpling before microelectrode insertion. Different locations within the lumbar enlargement were electrically stimulated to map the locomotor networks. The remaining 3 YMPs served as sham controls, receiving the laminectomy, durotomy, and pial cuts but not microelectrode insertion. The Porcine Thoracic Injury Behavioral Scale (PTIBS) and hindlimb reflex assessment results were recorded for 4 weeks postoperatively. Overground gait kinematics and hindlimb EMG activity were recorded again at weeks 3 and 4 postoperatively and compared with preoperative measures. The animals were euthanized at the end of week 4, and the lumbar spinal cords were extracted and preserved for immunohistochemical analysis.

RESULTS All YMPs showed transient deficits in hindlimb function postoperatively. Except for 1 YMP in the experimental group, all animals regained normal ambulation and balance (PTIBS score 10) at the end of weeks 3 and 4. One animal in the experimental group showed gait and balance deficits by week 4 (PTIBS score 4). This animal was excluded from the kinematics and EMG analyses. Overground gait kinematic measures and EMG activity showed no significant ($p > 0.05$) differences between preoperative and postoperative values, and between the experimental and sham groups. Less than 5% of electrode tracks were visible in the tissue analysis of the animals in the experimental group. There was no statistically significant difference in damage caused by pial cuts between the experimental and sham groups. Tissue damage due to the pial cuts was more frequently observed in immunohistochemical analyses than microelectrode tracks.

CONCLUSIONS These findings suggest that mapping spinal locomotor networks in porcine models can be performed safely, without lasting damage to the spinal cord.

https://thejns.org/doi/abs/10.3171/2024.2.SPINE23757

KEYWORDS intradural; kinematics; electromyography; electrical stimulation; locomotion; diagnostic technique

ABBREVIATIONS BF = biceps femoris; EMG = electromyographic; GM = gluteus medius; MTP = metatarsophalangeal; PTIBS = Porcine Thoracic Injury Behavioral Scale; ROM = range of motion; SCI = spinal cord injury; SCS = spinal cord stimulation; VL = vastus lateralis; YMP = Yucatan minipig.

SUBMITTED July 8, 2023. **ACCEPTED** February 21, 2024.
INCLUDE WHEN CITING Published online May 10, 2024; DOI: 10.3171/2024.2.SPINE23757.

* S.M. and C.L.O. contributed equally to this work and share first authorship.

Spinal cord injury (SCI) is a devastating neurological condition that is sustained by 250,000–500,000 individuals worldwide each year.[1] Regaining the ability to walk after SCI is consistently rated as one of the highest priorities by individuals with SCI.[2] It is well established that in mammals, the neuronal networks that produce motor synergies are in the spinal cord.[3] These networks below the level of injury can be reactivated by electrical stimulation.[4] The effectiveness of spinal cord stimulation (SCS) for restoring standing and stepping after SCI has been demonstrated in both animal models[5–9] and humans.[10–12] Although clinical trials of epidural SCS have shown promising results, the spatiotemporal activation patterns of locomotor networks continue to be guided by indirect measures including approximate myotomal maps or computational models.[10,13,14] Recruiting the most effective locomotor circuity while limiting the activation of less relevant neural networks requires optimization of stimulation targets, electrode configuration, and stimulation parameters. Understanding the functional organization of motor networks located deep in the spinal cord is essential for achieving specificity and optimal spinal neuromodulation. The topographical functional maps of the motor networks are available for the rat,[15] cat,[16] pig,[17] and rhesus monkey.[18] However, the functional map and stimulation amplitudes required for activating different locomotor circuits in the human spinal cord remain unknown. Therefore, a safe method for intraspinal mapping of locomotor networks in the spinal cord of humans is needed for obtaining the best outcomes with novel SCS techniques.

The anatomical and physiological similarities between humans and pigs have made the pig a practical model, especially in spinal cord–related studies.[19] In addition, comparative studies have demonstrated high similarities between the gross anatomy of the spine and spinal cord between pigs and humans.[20] More importantly, unlike most preclinical models, the pig spinal cord has a large subarachnoid space that is similar to that in humans.[21,22] This makes the pig a relevant model for preclinical testing of extra- and intradural interventions aimed at restoring mobility after neural injury or disease. Adult miniature pigs such as Yucatan minipigs (YMPs) have recently become widely used for biomedical and neuromodulation therapeutic studies especially related to SCI.[22,23]

Understanding the potential sensorimotor deficits resulting from direct spinal cord mapping using penetrating electrodes is crucial for designing a safe mapping procedure. In the current study, we evaluated the safety of mapping the locomotor networks in the spinal cord of YMPs by comparing the gait parameters and electromyographic (EMG) activity of YMPs before and after intraspinal mapping and through postmortem immunohistochemical analyses.

Methods

Surgical Procedure

A total of 11 YMPs were used in these experiments. All animal procedures were approved by the Animal Care and Use Committee at the University of Alberta. Prior to the surgical mapping procedure, the pigs were trained using positive reinforcement to walk up and down a 3.5-m straight walkway. Gait kinematics were captured using a reflective marker–based motion capture system (150 frames/sec, Vicon Motion Systems Ltd.) (Fig. 1A and B), and EMG data were recorded using a wireless surface EMG system (3000 Hz; Noraxon).

On the mapping day, the pigs were sedated and aseptically prepared for surgery. The total intravenous anesthesia protocol described in our previous work[24] was used to maintain anesthesia and consisted of a constant infusion of propofol (40–145 μg/kg/min), remifentanil (0.03–0.14 μg/kg/min), lidocaine (fixed dosage: 1.0 mg/kg/hr), and dexmedetomidine (fixed dosage: 0.2 μg/kg/hr). Spinal cord segments L4–6 (lumbar enlargement) were exposed, and the dura mater was incised. An ultrasound-guided stereotactic frame[25] was used to guide a platinum-iridium (80%/20%) microelectrode (125 μm, FHC Inc.) as it penetrated the spinal cord to map the locomotor networks in the intermediate and ventral gray matter (Fig. 1C).

To reduce the indentation of the spinal cord during microelectrode insertion, a small pial cut was made using an arachnoid knife. In 8 experimental animals, up to 12 penetrations were made across the lumbar enlargement with the microelectrode tips advancing 3.0–4.5 mm into one side of the spinal cord. Trains of 1-second-long electrical stimuli (200-μsec biphasic charge-balanced pulses, 40 Hz, 5–100 μA) were delivered at each location, and the evoked hindlimb movements were documented (Fig. 1D). In 3 sham control animals, 12 pial cuts were made on one side of the spinal cord but no microelectrode penetrations or stimulation occurred. The mapping procedure was limited to 2 hours to mimic a realistic duration for an intraoperative experimental procedure in humans. After microelectrode removal, dura mater and surgical wounds were sutured closed in layers and the animals recovered from anesthesia.

Postsurgical Care and Data Collection

Injectable and oral analgesics and antibiotics were administered for a minimum of 2 weeks postsurgery (see Supplemental Material for drugs and doses). Animals were frequently repositioned to reduce the risk of pressure injuries. Each week for 4 weeks after the surgical procedure, the Porcine Thoracic Injury Behavioral Scale (PTIBS; a 10-point scale that describes the recovery process of hindlimb function[22]) scores, as well as the presence and relative magnitude of the panniculus, perineal, and withdrawal reflexes in the hindlimbs, were evaluated. Kinematic and EMG data were recorded during the 3rd and 4th weeks postoperatively.

After 4 weeks, the pigs were anesthetized with isoflurane and the mapped region of the spinal cord was reexposed. Spinal cord segments (L4–6) were identified based on the location of dorsal rootlets. The pigs were euthanized with Euthanyl (Bimeda-MTC; 100 mg/kg), and the lumbar enlargement was removed and placed in 4% paraformaldehyde in 0.1 M phosphate buffer (PB) for 48 hours at 4°C, cryoprotected in increasing concentrations of sucrose (10%–30%) in 0.1M PB for 72 hours at 4°C, frozen on isopentane, and stored at −80°C.

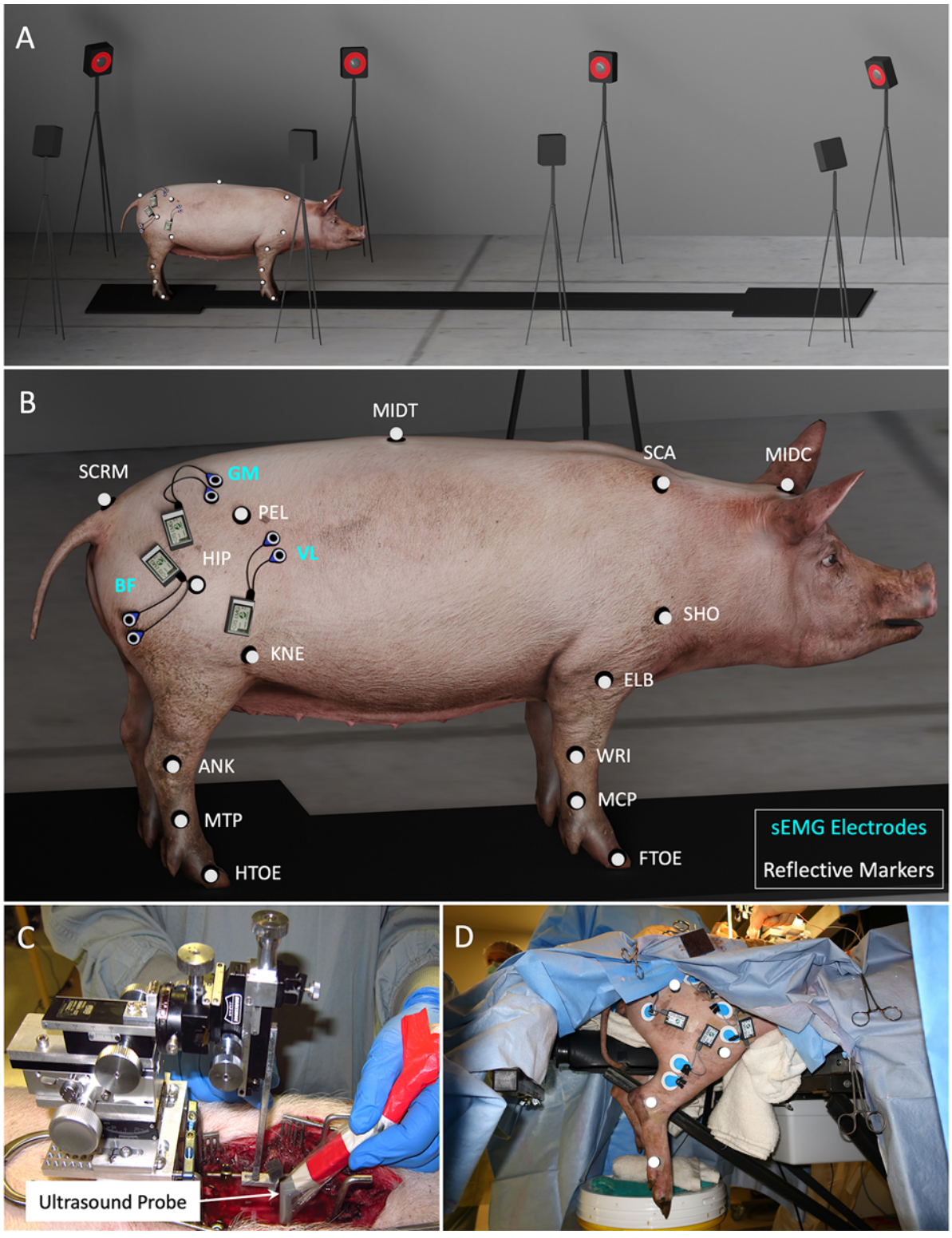

FIG. 1. A: Schematic image of the motion capture set up showing the 3.5-m walkway and 8 Vicon cameras. **B:** The position of different reflective markers and surface EMG (sEMG) electrodes on the joints and body. **C:** Stereotactic frame mounted on four lumbar pedicle screws used for insertion of microelectrodes with micromanipulators. **D:** Reflective markers and EMG electrodes attached to the skin over various joints and muscles to document movements during the mapping procedure. Hindlimbs were hung freely to capture the kinematic and EMG activity of evoked movements. ANK = ankle; ELB = elbow; FTOE = foretoe; HIP = hip; HTOE = hindtoe; KNE = knee; MCP = metacarpophalangeal; MIDC = midcervical; MIDT = midthoracic; PEL = pelvis; SCA = scapula; SCRM = sacrum; SHO = shoulder; WRI = wrist. Figure is available in color online only.

Kinematic and EMG Analysis

Motion capture and EMG data were processed using a sequence of custom-developed MATLAB programs (R2020b, The MathWorks, Inc.) as previously described.[26] Briefly, strides and the associated gait kinematic parameters (Supplemental Table 1) were sorted into 5 overground walking speed ranges (0.4–0.59, 0.6–0.79, 0.8–0.99, 1.0–1.19, and 1.2–1.4 m/sec). Each parameter at a speed range was compared between the experimental and sham groups before and after the operation. For intralimb coordination, the area and regularity of the joint-joint cyclograms were calculated to evaluate step repeatability.[27] Interlimb coordination for each animal was analyzed by calculating the overlap between the steps of the 4 limbs during a stride.[28]

EMG data for the left and right biceps femoris (BF), vastus lateralis (VL), and gluteus medius (GM) muscles were bandpass filtered (10–450 Hz), full-wave rectified, and low-pass filtered at 10 Hz. A common trigger was captured by the EMG and kinematic recording systems and was used to synchronize the data. EMG data for each stride were sorted into one of the 5 stride speed ranges. Outlier removal and inclusion criteria were chosen for kinematics and EMG data as previously explained.[26]

The mean EMG activity within the 0.8- to 0.99-m/sec speed range was assessed further to determine EMG burst onset and offset points within the gait cycle. An activation threshold was defined based on a region of low muscle activity (mean + 1.5 SD) for each YMP.[26,29] The onset and offset points of all pigs for each muscle were then averaged and compared.

Histological and Immunohistochemical Analyses

The frozen spinal cord blocks were cryosectioned at 20 μm, mounted on SuperFrost Plus slides (Fisher Scientific), dried for 30 minutes at room temperature, and stored at −80°C. Sections every 100 μm were stained with Harris H&E (Sigma-Aldrich Ltd.). Astrocytes were identified using a polyclonal primary GFAP antibody (anti–rabbit antibody; DAKO, Agilent Technologies Inc.) and activated microglia were identified using a polyclonal Iba1 antibody (anti–rabbit antibody, Abcam). Nuclei on all sections were stained with DAPI (Invitrogen, Thermo Fisher Scientific). For detailed staining protocol and list of antibodies used and their dilutions, see Supplemental Material.

Statistical Analysis

The swing time, stance time, and stride length were statistically analyzed between preoperative and postoperative conditions, and experimental and sham control groups for 5 speed ranges (speed factor) using three-way repeated-measures ANOVA (Prism version 9.3.1, GraphPad). A mixed-effects model was fitted to the data to handle the missing values for the joint angles; hoof and toe clearances; pelvic vertical displacements; homolateral, homologous, and diagonal interlimb coupling; and the area and regularity of the cyclograms for intralimb coordination. Mauchly's sphericity test was performed for each dataset, and the Greenhouse-Geisser correction was applied in case the sphericity assumption was violated. Tukey's honest significant difference post hoc test was used for multiple comparisons on all possible pairs of group means; $p \leq 0.05$ indicated a statistically significant difference. The Mann-Whitney rank-sum test was run for immunohistochemical analysis to compare the damaged tissue area between groups.

Results

Assessment of Behavioral Recovery and Reflexes

One animal in the sham group showed mild hindlimb deficits (PTIBS score 4), and 2 other animals showed plantar hoof placement with trunk imbalance while walking (PTIBS score 9) 1 week after surgery (Fig. 2A). All 3 animals in the sham group showed normal hindlimb walking from the 2nd week onward. Generally, animals in the sham group recovered 1 week sooner than animals in the experimental group. All animals in the experimental group showed normal hindlimb function by the end of week 4, except for 1 animal that did not score higher than 4 on the PTIBS scale (Fig. 2A). This animal was not able to walk without support and therefore was excluded from the subsequent kinematic analyses.

The presence or absence of 3 different reflexes was used to assess the integrity of sensorimotor pathways in the spinal cord. The perineal reflex was present with no changes in both the experimental and sham control groups throughout the 4-week postoperative testing. The panniculus reflex was reduced during the 1st week postoperatively for all animals but returned to normal magnitude thereafter. The withdrawal reflex was reduced for 2 weeks and 3 weeks postoperatively for the sham and experimental groups, respectively, and then recovered to normal (Fig. 2B).

Effect of the Mapping Procedure on Overground Walking Kinematics

Representative examples of the left and right hip, knee, and ankle joint angles for 1 experimental animal and 1 sham group animal before and after surgery are shown in Fig. 3A for all strides within the 0.60- to 0.79-m/sec speed range. These examples show that the general shape of the joint angles and ranges of motion (ROMs) were similar preoperatively and postoperatively. The mean and standard error of the joint angle ROMs at 5 different overground walking speed ranges are shown in Fig. 3B. Significant differences were found between preoperative and postoperative hip minimum and maximum angles as well as the ankle maximum angle ($p = 0.009$, $p = 0.008$, and $p = 0.027$, respectively) (Supplemental Table 1). No other significant differences were found between preoperative and postoperative or experimental and sham groups for any of the other evaluated parameters (maximum, minimum, ROM, time of maximum, and time of minimum joint angles) for the hip, knee, and ankle joint angles ($p = 0.124$). Post hoc comparisons showed no statistically significant differences ($p > 0.163$) within each range of walking speed (Supplemental Fig. 1).

Examples of pre- and postoperative vertical displacements of the pelvis, hindtoe, and metatarsophalangeal (MTP) markers above the ground in a gait cycle at 0.6- to 0.79-m/sec for 1 experimental animal and 1 sham group animal before and after surgery are shown in Fig. 4A. The mean and standard error of the vertical displacement for

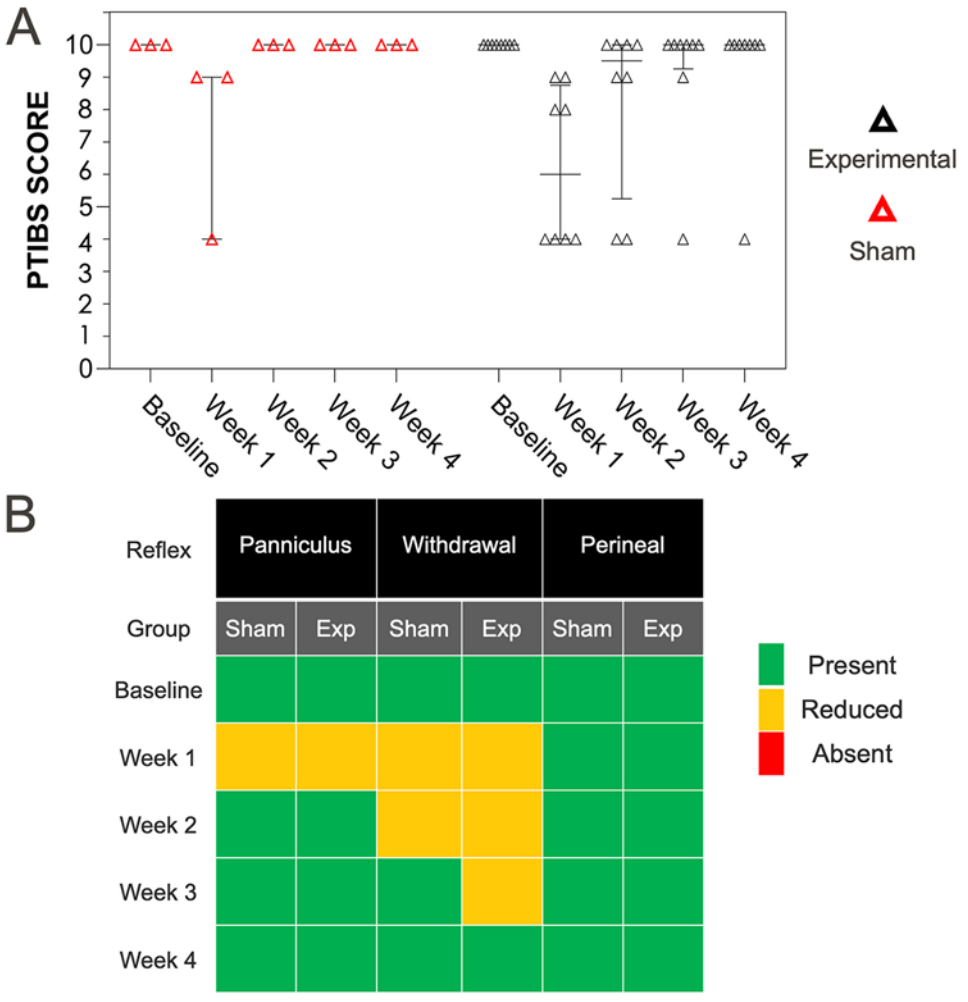

FIG. 2. A: PTIBS scores documented for animals in the sham and experimental groups. A score of 10 represents grossly normal ambulation with normal balance. A score of 9 describes an animal that can take more than 6 steps with fully extended knees, plantar hoof placement, and trunk imbalance. A score of 8 describes an animal that can take more than 6 steps with knees fully extended, plantar or dorsal hoof placement, and impaired balance during walking. A score of 4 represents active rhythmic hindlimb crawling with at least 3 reciprocating gait cycles; rump off the ground with transient weight-bearing extensions. **B:** Present, reduced, or absent reflexes recorded preoperative and weekly for 4 weeks postoperative for animals in the sham and experimental (exp) groups. Figure is available in color online only.

the pelvis, toe, and MTP joints in a gait cycle are shown in Fig. 4B for experimental and sham animals before and after surgery for 5 speed ranges. There were no differences between the groups for pelvic height and MTP clearance ($p > 0.05$) (Fig. 4). The toe markers fell off frequently and resulted in small sample sizes; therefore, no statistical test was performed for hindtoe clearance.

Except for the time of maximum hip angle, significant differences were seen for all joint angle parameters and pelvic height with increasing walking speeds within each group as previously observed[26] (Supplemental Table 1).

Interlimb coordination for 5 speed ranges are shown in Fig. 5A as polar plots for left forelimb versus right hindlimb (diagonal), left forelimb versus left hindlimb (homolateral), and left forelimb versus right forelimb (homologous). No statistically significant differences were found between preoperative versus postoperative and experimental versus sham groups. Changes in overground walking speed showed significant differences in the diagonal and homolateral couplings within each group ($p < 0.05$) (Supplemental Table 1). A transition in the gait pattern form lateral to diagonal stepping sequence was observed at around 1 m/sec in all 4 groups (Fig. 5, Supplemental Table 1).

The variations in swing time, stance time, and stride length across the experimental and sham groups pre- and postoperatively for the averaged data within 5 speed ranges and for all recorded strides are shown in Fig. 6A and Fig. 6B, respectively. There were no significant differences between the groups in the swing time, stance time, and stride length within each speed range (Fig. 6A). However, the swing and stance time decreased, and the stride length increased significantly with increasing walking speed within each group as expected[26] ($p < 0.05$) (Supplemental Table 1).

Second-order polynomial and exponential growth curves were fitted to the swing and stance time, respectively (Fig. 6B). In the experimental group, the fitted curves

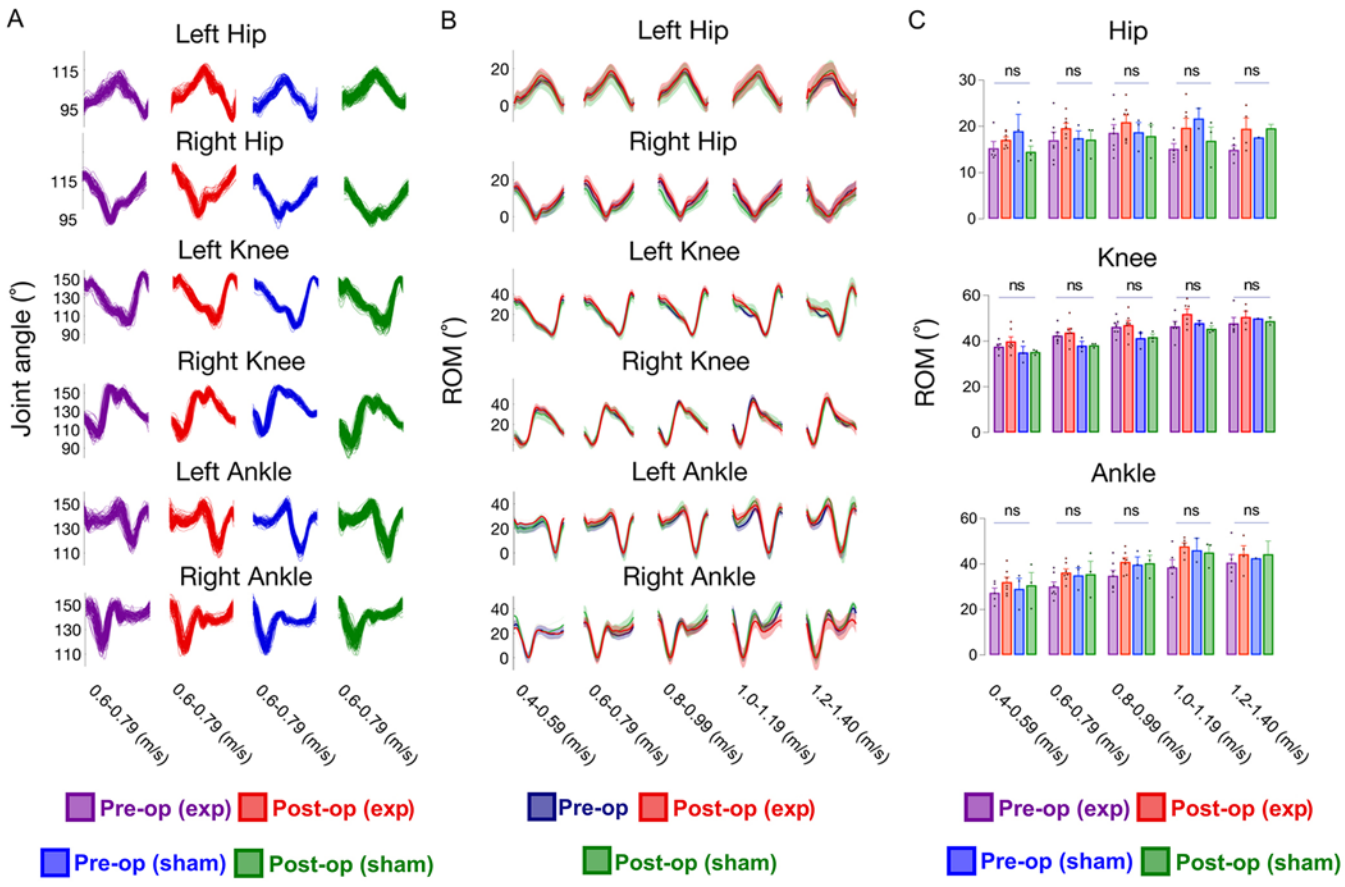

FIG. 3. A: Example of left and right hip, knee, and ankle joint angles calculated in a gait cycle for different animal groups (preoperative experimental [ex], postoperative experimental, preoperative sham, and postoperative sham) at an overground walking speed of 0.6 to 0.79 m/sec. **B:** Means (*solid line*) and standard errors (*shaded area*) of left and right joint angle ROM are shown for preoperative (all animals) and postoperative for animals in the experimental (n = 7) and sham control (n = 3) groups at 5 different overground walking speed ranges. **C:** Means and standard errors of hip, knee, and ankle ROMs at various overground walking speed ranges for all animal groups (preoperative experimental, postoperative experimental, preoperative sham, postoperative sham). ns = not significant. Figure is available in color online only.

for stance time were identical pre- and postoperatively, while in the sham group, they were closely matched. For swing time, fitted curves in both sham and experimental groups were highly similar pre- and postoperative, though not entirely identical.

The average cyclograms are demonstrated in Supplemental Fig. 2 for experimental and shame groups pre- and postoperatively at 5 speed ranges. No statistically significant differences were found between the groups for the area and regularity of the cyclograms at each speed range (Supplemental Fig. 3, Supplemental Table 1).

Activity of Hindlimb Muscles

The representative example of pre- and postoperative EMG activity from 1 YMP with stride speeds between 0.8 and 0.99 m/sec in Fig. 7A demonstrates how bursts of activity were detected. For the BF, VL, and GM muscles, primary peaks were typically centered around 15% and 65% of the gait cycle for the left and right legs, respectively. In some cases, 2 or 3 distinct bursts were detected, such as for the left BF and right GM muscles (Fig. 7B). Secondary or tertiary bursts did not occur consistently at the same points during the gait cycle; therefore, only primary bursts were characterized. Because of insufficient data for some animals, muscle activation patterns were calculated based on fewer animals. The average EMG onset and offset points for all muscles of the animals in the 4 groups are shown in Fig. 7C. Overall, there were no significant differences between any groups for the muscle onset and offset points. On average, the BF muscle exhibited activity between 3% and 25% and between 45% and 72% of the gait cycle for the left and right legs, respectively. Similarly, the VL displayed activity between 3% and 23% and between 48% and 71% of the gait cycle for the left and right legs, respectively. Lastly, the left GM muscle exhibited a burst of activity between 5% and 22% and between 51% and 73% of the gait cycle for the left and right legs, respectively.

Histological and Immunohistochemical Analyses

Histochemical analyses revealed that of the 8–12 microelectrode insertions in each of the 8 experimental pigs, only 3 electrode tracks were visible in the serial cross-sections. There was no significant difference in the volume of tissue damaged by pial cuts between sham control and experi-

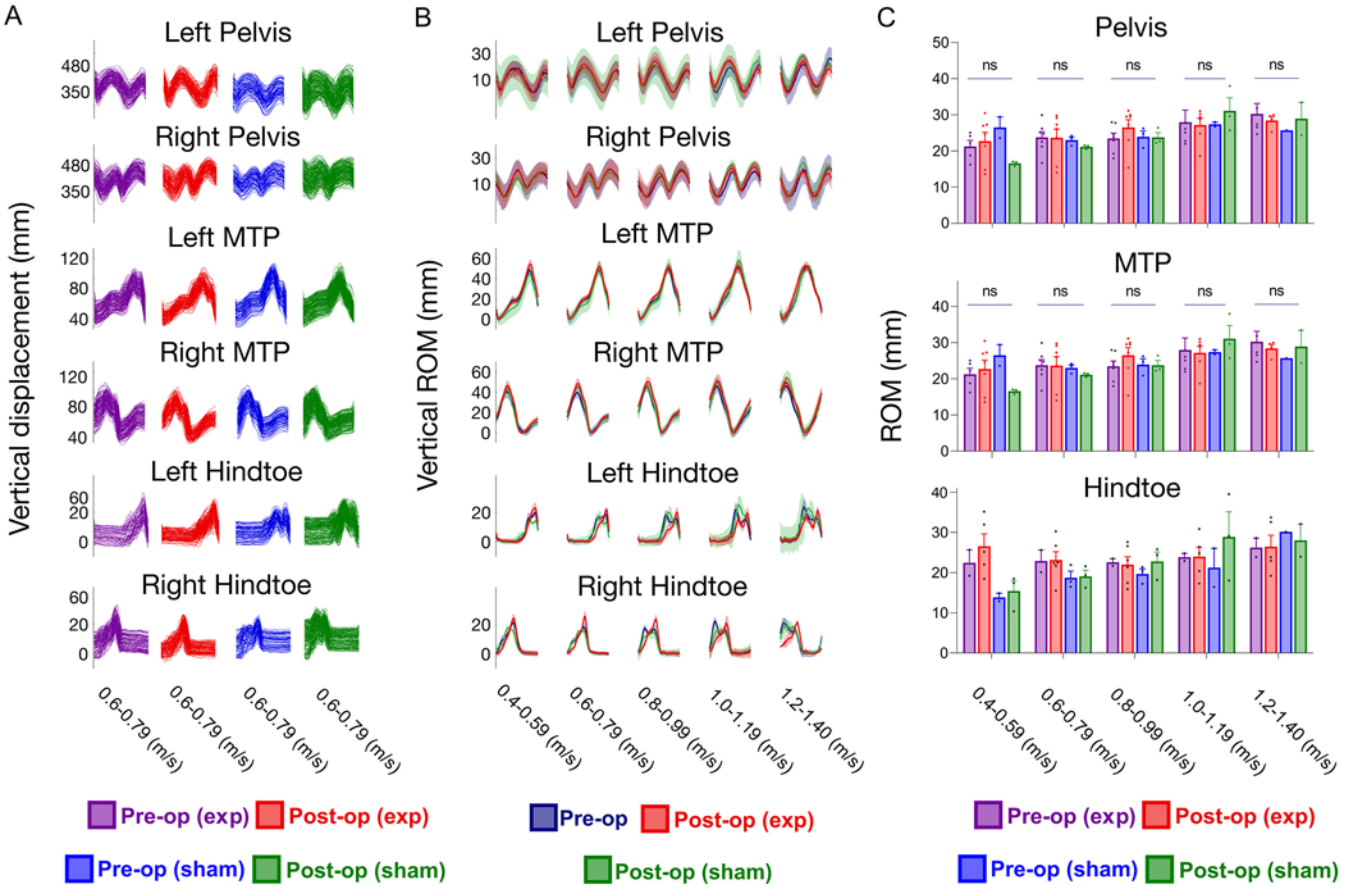

FIG. 4. A: Examples of left and right pelvis, MTP, and hindtoe vertical displacement for 1 animal in the experimental and 1 in the sham group pre- and postsurgery at 0.6–0.79 m/sec. **B:** Means (*solid line*) and standard errors (*shaded area*) of left and right pelvis, MTP, and hindtoe vertical displacement are shown preoperatively (all animals) and postoperatively for animals in the experimental (n = 5) and sham control (n = 3) groups at 5 different overground walking-speed ranges. **C:** Comparisons of vertical ROMs of pelvis, MTP, and hind toe joints between the 4 groups (preoperative experimental, postoperative experimental, preoperative sham, and postoperative sham) at 5 speed ranges. Individual points show mean values obtained from each animal. Because of the small sample sizes for hindtoe, statistical comparisons were not performed. Figure is available in color online only.

mental groups ($p = 0.467$). The average volume of damage measured across the microelectrode tracks and pial cuts in the experimental group and of pial cuts in the sham control group were 0.79 ± 0.48 mm^3 (0.48% of the L4 spinal cord segment and 0.21% of L5 spinal cord segment volumes), 0.98 ± 0.22 mm^3 (0.49% of the L4 spinal cord segment, 2.32% of the L5 spinal cord segment, and 0.77% of the L6 spinal cord segment volumes), and 0.40 ± 0.07 mm^3 (0.08% of the L4 spinal cord segment, 0.68% of the L5 spinal cord segment, and 0.31% of the L6 spinal cord segment volumes), respectively (Fig. 8Q). Immunohistochemical data showed astrocytes encapsulating the area of damage from the microelectrode tracks (Fig. 8A–H) and the pial cuts (Fig. 8I–P). Activated microglia were also visible in the damaged area that was encapsulated by astrocytes.

Discussion

Neural circuits in the spinal cord integrate descending commands and sensory inputs to generate complex motor outputs.[30] Electrical stimulation of intraspinal networks in animal models using penetrating electrodes generates coordinated motor synergies with higher selectivity and less electrical current compared with epidural stimulation.[6,31,32] Mapping these networks in humans provides valuable information about the functional organization of neuronal circuits that generate coordinated muscle synergies using electrical neuromodulation. This knowledge can guide the design of devices aiming to restore locomotion after severe SCI in humans.

This study aimed to investigate the safety of using penetrating stimulation electrodes for mapping the functional organization of motor synergies within the lumbar spinal cord in a clinically translational animal model, YMPs. A range of measures including behavioral assessments, kinematics, muscle activity, and immunohistochemical analysis were used in this evaluation. All animals successfully recovered from the mapping operation without encountering infection, dural defects, or subdural/subcutaneous hematoma or seroma, although these complications have been relatively infrequent.[33,34] PTIBS scores showed transient, early deficits except for 1 animal in the experimental group that showed gait and balance problems. This animal was unable to walk without balance support up to 4 weeks

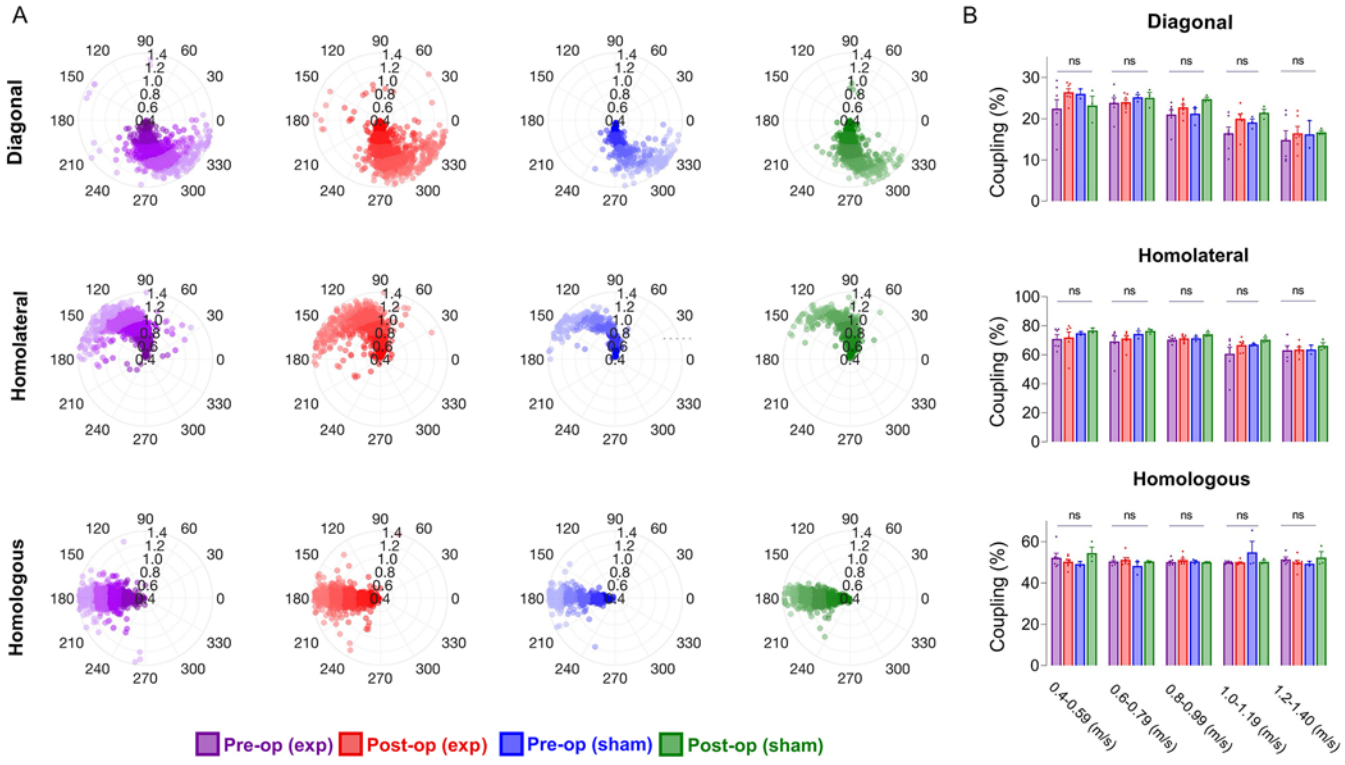

FIG. 5. A: Diagonal, lateral, and homologous coupling values shown in polar plots for different animal groups (preoperative experimental, postoperative experimental, preoperative sham, and postoperative sham) at 5 overground walking-speed ranges. Diagonal coupling: left forelimb versus right hindlimb; homolateral coupling: left forelimb versus left hindlimb; homologous coupling: left forelimb versus right forelimb. The angle of each point shown in the polar plots represents the phase angle difference between the gait cycle of different limbs as percentage of the perimeter of the circles in the counterclockwise direction, while the radius of each point represents the walking speed in that stride. **B:** Mean and standard error of diagonal, homolateral, and homologous coupling and statistical comparisons between the 4 groups (preoperative experimental, postoperative experimental, preoperative sham, and postoperative sham) at 5 overground walking-speed ranges. No statistically significant differences were seen between any of the coupling values at each speed range. Figure is available in color online only.

postoperatively. The postmortem analysis of spinal cord tissue for this animal did not reveal any abnormal tissue damage (Supplemental Fig. 4), and as such the cause of these differences remains unknown. It is possible that the postoperative analgesics caused this animal to experience nausea that compromised its ability to balance, a known side effect of the same analgesics in humans. Otherwise, the deficits observed in this animal may be associated with other unidentified nonneurological or spinal cord surgery–related changes.

For all other experimental animals, only 3 of 36 evaluated kinematic measures showed statistically significant differences between preoperative and postoperative conditions, but none between the experimental and sham control groups. The hip maximum and minimum angles showed significant increases after surgery (Supplemental Table 1); however, the hip ROM remained unchanged, suggesting that the changes in the hip minimum and maximum angles might be caused by an inconsistency in the placement of reflective markers pre- and postoperatively. Collectively, these results together with the PTIBS scores and reflex assessments show the integrity of sensorimotor networks in the spinal cord following the acute insertion and stimulation through penetrating microelectrodes intraoperatively.

In a recent study, 6 juvenile pigs recovered successfully after implantation of intradural spinal cord stimulating devices through a 1-level laminectomy.[35] In the current study, a 2- to 3-level laminectomy was performed. It has been suggested that spinal fixation after multiple-level interlaminar decompression surgery and durotomy in porcine models can prevent postoperative SCI and neurological deficits.[36] Nonetheless, spinal fixation did not appear to be a necessary adjunct to the mapping procedure used in this study.

Microelectrode insertion in the neural tissue can damage neurons and glia, disrupt the neurovasculature, and increase blood-brain barrier permeability. This causes infiltration of neutrophils and upregulation of proinflammatory cytokines such as interlukin-1β and interleukin-6, which can activated resident microglia.[37,38] Proinflammatory microglia extend their processes toward an implanted device within 45 minutes postimplantation.[38] In vivo imaging studies have demonstrated that acute insertion of neural probes in the visual cortex in mice causes mechanical deformation of cells leading to altered morphology of the subcellular compartments.[39] Also, higher calcium levels in neuronal soma and neurites were observed within 150 μm in the vicinity of microelectrodes following implantation, but returned to normal after 28 days postinsertion.[38,39]

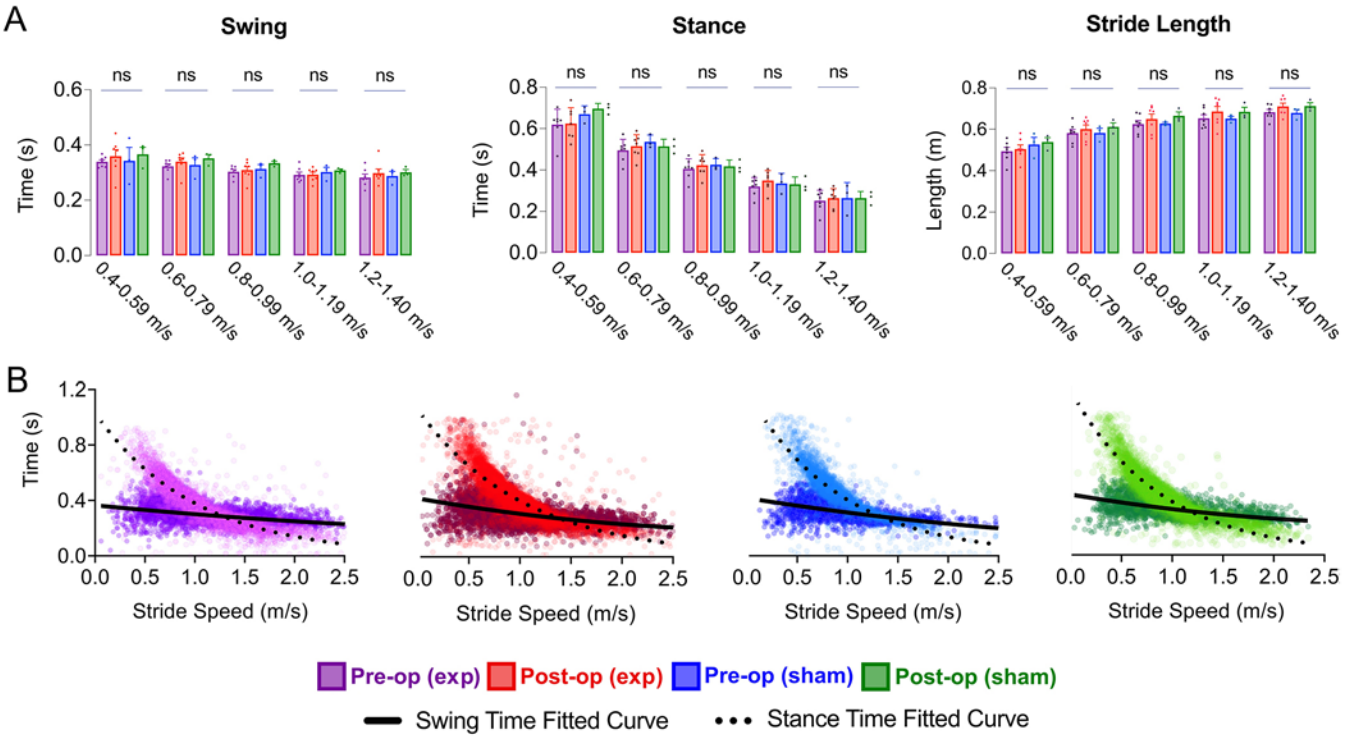

FIG. 6. A: Comparisons of swing and stance time and stride length between the four groups (preoperative experimental, postoperative experimental, preoperative sham, and postoperative sham) at 5 speed ranges. **B:** Swing and stance times plotted as a function of stride speed for the 4 groups. The fitted curves for stance time preoperatively and postoperatively for the experimental group were $y = 1.03e^{(-1.0x)}$ (n = 7287, r = 0.86) and $y = 1.03e^{(-1.0x)}$ (n = 6925, r = 0.79), respectively, and the fitted curves for stance time preoperatively and postoperatively in the sham group were $y = 1.18e^{(-1.1x)}$ (n = 3770, r = 0.85) and $y = 1.17e^{(-1.1x)}$ (n = 3919, r = 0.89), respectively. The fitted curves for swing time preoperatively and postoperatively for the experimental group were $y = 0.36 - 0.07x + 0.006x^2$ (n = 7319, r = 0.45) and $y = 0.41 - 0.13x + 0.017x^2$ (n = 9883, r = 0.46), and the fitted curves for swing time preoperatively and postoperatively for the sham group were $y = 0.41 - 0.11x + 0.011x^2$ (n = 3777, r = 0.53) and $y = 0.43 - 0.12x + 0.018x^2$ (n = 3940, r = 0.49), respectively. The preoperative and postoperative fitted curves were not significantly different from each other for the experimental or the sham group. These fitted curves for the experimental and sham groups were also not significantly different from each other. Figure is available in color online only.

Cats implanted with microelectrodes in their spinal cord for 6 months showed either no neurological deficits or transient paresis recovering within two weeks.[40] A study in rats did not find a decrease in neuronal cell bodies around penetrating microelectrodes after stimulating the tissue for 4 hours/day for 30 days.[41] An increase in density of immunoreactive astrocytes and microglia (confined to 200 μm) was seen around both the stimulating and nonstimulating implanted microelectrodes.[41] Notably, in those studies,[40,41] the microelectrodes were chronically implanted in the tissue. In the present study, the microelectrodes were acutely inserted in the spinal cord for 2 hours to electrically stimulate the cord before removal from the tissue. Biran et al.,[42] observed an increase in microglia and astrocytes and a decline in neuronal density and neurofilament in the vicinity of implanted silicon electrodes in the rat cortex after 4 weeks. In contrast, brain tissue subjected to stab wounds created by the same electrodes showed no reduction in neurofilament immunoreactivity and neuronal density, and significant reduction in $ED1^+$ and GFAP immunoreactivity by 4 weeks, making it difficult to locate the wounds in the tissue.[42]

In the current study, immunohistochemical analysis of extracted spinal cords showed electrode tracks containing astrocytes and glial cells in less than 5% of the electrode insertion sites. This implies that the tissue damage caused by acute microelectrode implantation and charge delivery during electrical stimulation was not enough to stimulate gliosis and scar formation in most cases. Furthermore, no proinflammatory macrophages were observed in the immunohistochemical images, indicating that any invasion across the blood-brain barrier was no longer present by week 4 postsurgery.

Although no significant differences were found in the volume of the scar tissue formed by pial cuts and microelectrode insertions, higher instances of pial cut-associated damage were found in the spinal cord tissue. Pial cuts were made to reduce spinal cord compression during electrode insertion. The diameter of the microelectrode significantly affects the tissue compression formed before pial rupture, the initial insertion force, and the force required for further insertion of the electrode in the neural tissue.[43] Using smaller diameter microelectrodes reduces both the insertion force and potential damage caused by mechanical strain of neural tissue during penetration.[43] Previous experiments performed on domestic pigs in our group have shown successful insertion of 50-μm microelectrodes with

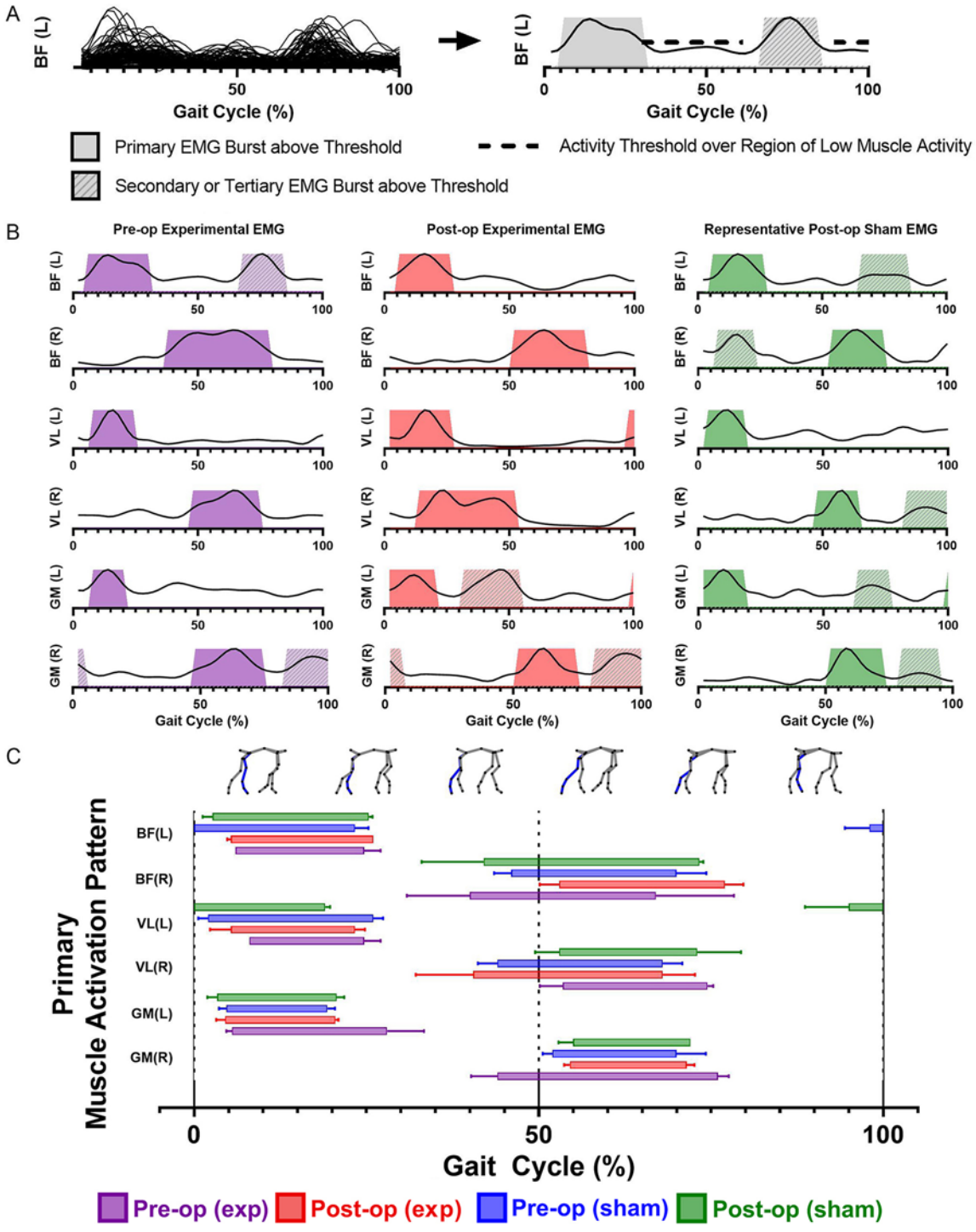

FIG. 7. A: An example of EMG activity recorded from 1 animal and the method for identifying primary and secondary bursts of muscle activity based on the defined threshold (mean + 1.5 SD). EMG bursts were identified when mean activity surpassed a threshold based on a specified low-activity region (region under the *black dashed line*) for each pig. In most cases, only one primary burst of EMG activity was observed, which was located at a consistent point in the gait cycle for all pigs. **B:** Mean EMG activities of left and right BF, VL, and GM muscles and their primary (*darker colors*) and secondary (*lighter colors*) burst of activity in a gait cycle for an animal in each of the preoperative and postoperative (experimental) and postoperative (sham) groups. **C:** The average and standard error of EMG onset and offset points of primary burst for left and right BF, VL, and GM muscles in a gait cycle for animals in the 4 groups (preoperative experimental; postoperative experimental; preoperative sham; postoperative sham). The number of animals included in EMG activity analysis is as follows: BF (left [L]): preoperative experimental, n = 4; preoperative sham, n = 3; postoperative experimental, n = 4; postoperative sham, n = 3. BF (right [R]): preoperative experimental, n = 5; preoperative sham, n = 3; postoperative experimental, n = 4; postoperative sham, n = 3. GM (L): preoperative experimental, n = 5; preoperative sham, n = 3; postoperative experimental, n = 4; postoperative sham, n = 3. GM (R): preoperative experimental, n = 5; preoperative sham, n = 2; postoperative experimental, n = 4; postoperative sham, n = 3. VL (L): preoperative experimental, n = 4; preoperative sham, n = 3; postoperative experimental, n = 4; postoperative sham, n = 3. VL (R): preoperative experimental, n = 5; preoperative sham, n = 3; postoperative experimental, n = 4; postoperative sham, n = 3. Figure is available in color online only.

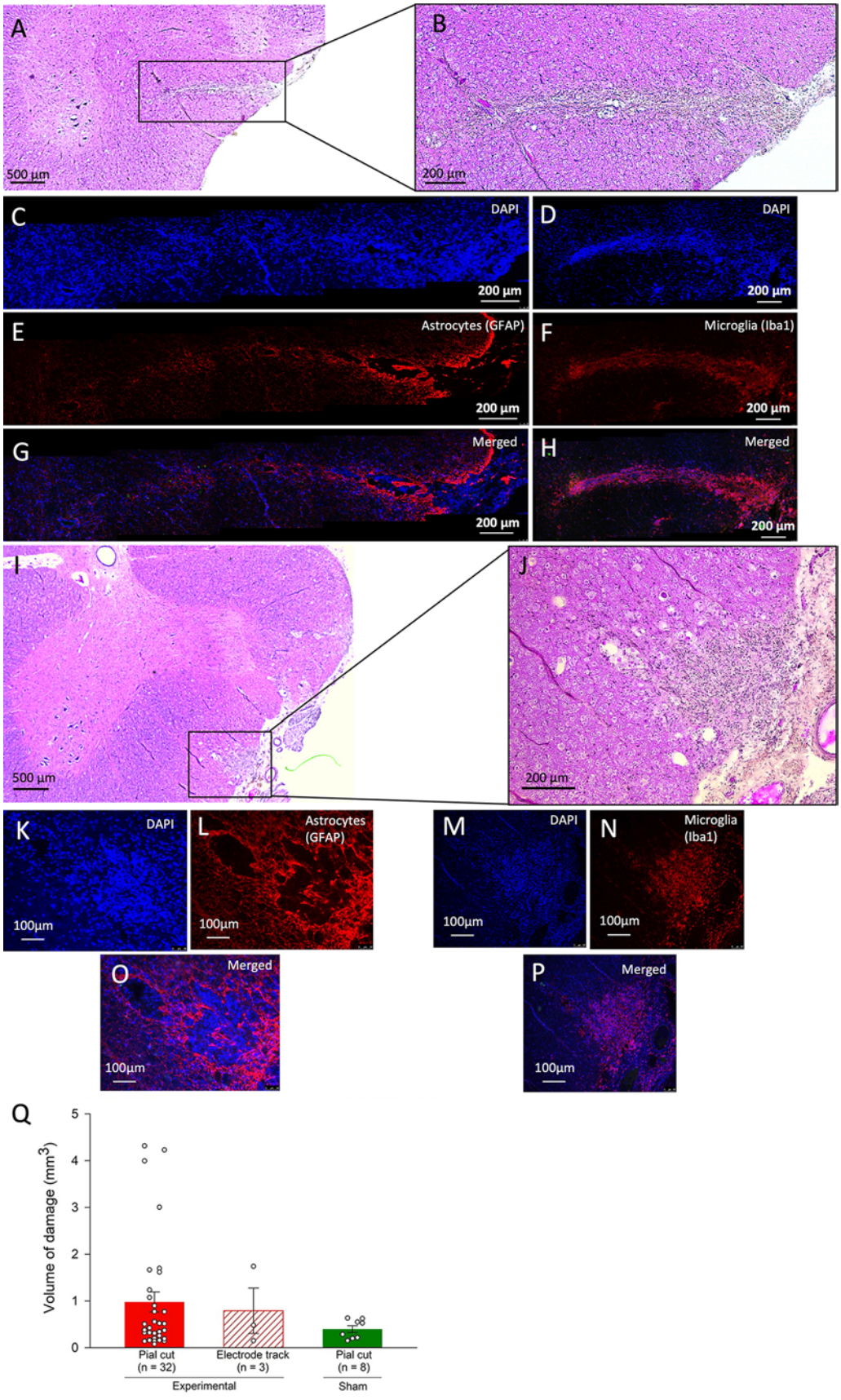

FIG. 8. A and B: Micrographs of spinal cord tissue stained with H&E showing an electrode track. **C–H:** Immunohistochemical images of the same electrode track stained with DAPI, GFAP, and Iba1 for labeling all cell nuclei, astrocytes, and microglial cells, respectively. **FIG. 8.** (*continued*)→

FIG. 8. I and J: An example of pial cut damage in a spinal cord tissue stained with H&E. **K–P:** Immunohistochemical images of the same pial cut damaged area stained with DAPI, GFAP, and Iba1 for labeling all cell nuclei, astrocytes, and microglial cells, respectively. **Q:** The mean and standard error of the volume of damaged tissue measured for pial cuts in the postoperative experimental and sham groups and electrode tracks in the postoperative experimental group. Figure is available in color online only.

beveled tips in the spinal cord without pial cuts, and without appreciable compression of the cord during insertion.[24] Moreover, pulsed laser ablation has been successfully tested to reduce the thickness of the pia mater and associated insertion force of electrodes in the sheep cortex.[44] In another study, ultrasonic microvibration was used to facilitate electrode insertion in the domestic pig cortex with an intact pia mater.[45] These methods can be implemented in the future to reduce the damage caused by pial cuts during electrode insertion in the spinal cord during functional mapping procedures using classic microelectrodes.

Limitations

Minor limitations were identified in the current study. We were constrained to using 125-μm microelectrodes with conical tips because of our preference for using commercially available, FDA-approved microelectrodes for the mapping procedure. Microelectrodes with smaller diameters and beveled tips would reduce tissue damage, especially by eliminating the need for pial cuts.[24] The recording of muscle activity was limited to muscles that can be reached via surface EMG recordings. Furthermore, force plates that provide quantified information about weight-bearing were not used in this study.

Conclusions

The findings suggest that despite transient deficits, function was nearly fully recovered in 7 of 8 experimental animals and all sham animals after 4 weeks. This suggests that negligible damage is caused by electrode insertion and stimulation; however, a less disruptive technique is needed for placing the pial cuts when using classic microelectrodes. These findings suggest that this approach is potentially a safe procedure to be used clinically for mapping the locomotor networks in humans. The intended clinical application involves conducting the mapping procedure concurrently with spinal cord surgery for individuals with severe SCI. The objective is to collect information regarding the location and organization of locomotor-related neural networks, thereby enhancing the precision of targeting locations for SCS and refining the interventions used for recovery of function after severe SCI.

Acknowledgments

This work was supported in part by the Canadian Institutes of Health Research (CIHR), Canada Foundation for Innovation, and US Department of Defense CDMRP-SCIRP. S.M. was supported by a Faculty of Medicine & Dentistry Dean's Doctoral Scholarship and an Alberta Innovates Health Solution Scholarship. C.L.O. and D.A.R. were supported by a Natural Sciences and Engineering Research Council Graduate Scholarship and an Alberta Graduate Excellence Scholarship. P.F. was supported by a University of Alberta Master's Entrance Scholarship and an Alberta Graduate Excellence Scholarship. D.S.H. was supported by a Faculty of Medicine & Dentistry Graduate Recruitment Scholarship and a Queen Elizabeth II Graduate Scholarship. A.T. was supported by a CIHR Vanier Canada Graduate Scholarship, an Alberta Innovates Health Solutions Studentship, and a Queen Elizabeth II Graduate Scholarship. V.K.M. is a Canada Research Chair (Tier 1) in Functional Restoration.

References

1. World Health Organization, International Spinal Cord Society. *International Perspectives on Spinal Cord Injury*. World Health Organization; 2013. Accessed March 7, 2024. https://iris.who.int/bitstream/handle/10665/94190/9789241564663_eng.pdf?sequence=1
2. Simpson LA, Eng JJ, Hsieh JT, Wolfe DL. The health and life priorities of individuals with spinal cord injury: a systematic review. *J Neurotrauma*. 2012;29(8):1548-1555.
3. Bizzi E, Giszter SF, Loeb E, Mussa-Ivaldi FA, Saltiel P. Modular organization of motor behavior in the frog's spinal cord. *Trends Neurosci*. 1995;18(10):442-446.
4. Capogrosso M, Wagner FB, Gandar J, et al. Configuration of electrical spinal cord stimulation through real-time processing of gait kinematics. *Nat Protoc*. 2018;13(9):2031-2061.
5. Dalrymple AN, Everaert DG, Hu DS, Mushahwar VK. A speed-adaptive intraspinal microstimulation controller to restore weight-bearing stepping in a spinal cord hemisection model. *J Neural Eng*. 2018;15(5):056023.
6. Holinski BJ, Mazurek KA, Everaert DG, et al. Intraspinal microstimulation produces over-ground walking in anesthetized cats. *J Neural Eng*. 2016;13(5):056016.
7. Saigal R, Renzi C, Mushahwar VK. Intraspinal microstimulation generates functional movements after spinal-cord injury. *IEEE Trans Neural Syst Rehabil Eng*. 2004;12(4):430-440.
8. Dalrymple AN, Mushahwar VK. Intelligent control of a spinal prosthesis to restore walking after neural injury: recent work and future possibilities. *J Med Robot Res*. 2020;5(01n02):2041003.
9. Dalrymple AN, Roszko DA, Sutton RS, Mushahwar VK. Pavlovian control of intraspinal microstimulation to produce over-ground walking. *J Neural Eng*. 2020;17(3):036002.
10. Rowald A, Komi S, Demesmaeker R, et al. Activity-dependent spinal cord neuromodulation rapidly restores trunk and leg motor functions after complete paralysis. *Nat Med*. 2022;28(2):260-271.
11. Angeli CA, Boakye M, Morton RA, et al. Recovery of overground walking after chronic motor complete spinal cord injury. *N Engl J Med*. 2018;379(13):1244-1250.
12. Gill ML, Grahn PJ, Calvert JS, et al. Neuromodulation of lumbosacral spinal networks enables independent stepping after complete paraplegia. *Nat Med*. 2018;24(11):1677-1682.
13. Hofstoetter US, Perret I, Bayart A, et al. Spinal motor mapping by epidural stimulation of lumbosacral posterior roots in humans. *iScience*. 2020;24(1):101930.
14. Darrow D, Balser D, Netoff TI, et al. Epidural spinal cord stimulation facilitates immediate restoration of dormant motor and autonomic supraspinal pathways after chronic neurologically complete spinal cord injury. *J Neurotrauma*. 2019;36(15):2325-2336.
15. Borrell JA, Frost SB, Peterson J, Nudo RJ. A 3D map of the hindlimb motor representation in the lumbar spinal cord in Sprague Dawley rats. *J Neural Eng*. 2017;14(1):016007.
16. Mushahwar VK, Horch KW. Selective activation of muscle groups in the feline hindlimb through electrical microstimulation of the ventral lumbo-sacral spinal cord. *IEEE Trans Rehabil Eng*. 2000;8(1):11-21.

17. Hachmann JT, Jeong JH, Grahn PJ, et al. Large animal model for development of functional restoration paradigms using epidural and intraspinal stimulation. *PLoS One*. 2013;8(12):e81443.
18. Toossi A, Everaert DG, Perlmutter SI, Mushahwar VK. Functional organization of motor networks in the lumbosacral spinal cord of non-human primates. *Sci Rep*. 2019;9(1):13539.
19. Kim KT, Streijger F, Manouchehri N, et al. Review of the UBC porcine model of traumatic spinal cord injury. *J Korean Neurosurg Soc*. 2018;61(5):539-547.
20. Toossi A, Bergin B, Marefatallah M, et al. Comparative neuroanatomy of the lumbosacral spinal cord of the rat, cat, pig, monkey, and human. *Sci Rep*. 2021;11(1):1955.
21. Noga BR, Santamaria AJ, Chang S, et al. The micropig model of neurosurgery and spinal cord injury in experiments of motor control. In: Whelan PJ, Sharpies SA, eds. *The Neural Control of Movement: Model Systems and Tools to Study Locomotor Function*. Elsevier; 2020:349-384.
22. Lee JH, Jones CF, Okon EB, et al. A novel porcine model of traumatic thoracic spinal cord injury. *J Neurotrauma*. 2013; 30(3):142-159.
23. Lim JH, Piedrahita JA, Jackson L, Ghashghaei T, Olby NJ. Development of a model of sacrocaudal spinal cord injury in cloned Yucatan minipigs for cellular transplantation research. *Cellular Reprogram*. 2010;12(6):689-697.
24. Toossi A, Everaert DG, Uwiera RRE, et al. Effect of anesthesia on motor responses evoked by spinal neural prostheses during intraoperative procedures. *J Neural Eng*. 2019;16(3):036003.
25. Toossi A, Everaert DG, Seres P, et al. Ultrasound-guided spinal stereotactic system for intraspinal implants. *J Neurosurg Spine*. 2018;29(3):292-305.
26. Mirkiani S, Roszko DA, O'Sullivan CL, et al. Overground gait kinematics and muscle activation patterns in the Yucatan mini pig. *J Neural Eng*. 2022;19(2):026009.
27. Tepavac D, Field-Fote EC. Vector coding: a technique for quantification of intersegmental coupling in multicyclic behaviors. *J Appl Biomech*. 2001;17(3):259-270.
28. Leblond H, L'Espérance M, Orsal D, Rossignol S. Treadmill locomotion in the intact and spinal mouse. *J Neurosci*. 2003; 23(36):11411-11419.
29. Courtine G, Roy RR, Hodgson J, et al. Kinematic and EMG determinants in quadrupedal locomotion of a non-human primate (Rhesus). *J Neurophysiol*. 2005;93(6):3127-3145.
30. Grillner S, El Manira A. Current principles of motor control, with special reference to vertebrate locomotion. *Physiol Rev*. 2020;100(1):271-320.
31. Sharpe AN, Jackson A. Upper-limb muscle responses to epidural, subdural and intraspinal stimulation of the cervical spinal cord. *J Neural Eng*. 2014;11(1):016005.
32. Tresch MC, Bizzi E. Responses to spinal microstimulation in the chronically spinalized rat and their relationship to spinal systems activated by low threshold cutaneous stimulation. *Exp Brain Res*. 1999;129(3):401-416.
33. Gakhar H, Bommireddy R, Klezl Z, Calthorpe D. Spinal subdural hematoma as a complication of spinal surgery: can it happen without dural tear? *Eur Spine J*. 2013;22(Suppl 3): S346-S349.
34. Dowdell J, Brochin R, Kim J, et al. Postoperative spine infection: diagnosis and management. *Global Spine J*. 2018;8(4 Suppl):37S-43S.
35. Holland MT, Seaman SC, Woodroffe RW, et al. In vivo testing of a prototype intradural spinal cord stimulator in a porcine model. *World Neurosurg*. 2020;137:e634-e641.
36. Slot EMH, de Boer B, Redegeld S, et al. Spinal fixation after laminectomy in pigs prevents postoperative spinal cord injury. *Animal Model Exp Med*. 2022;5(2):153-160.
37. Kozai TDY, Vazquez AL, Weaver CL, Kim SG, Cui XT. In vivo two-photon microscopy reveals immediate microglial reaction to implantation of microelectrode through extension of processes. *J Neural Eng*. 2012;9(6):066001.
38. Wellman SM, Kozai TDY. In vivo spatiotemporal dynamics of NG2 glia activity caused by neural electrode implantation. *Biomaterials*. 2018;164:121-133.
39. Eles JR, Vazquez AL, Kozai TDY, Cui XT. In vivo imaging of neuronal calcium during electrode implantation: spatial and temporal mapping of damage and recovery. *Biomaterials*. 2018;174:79-94.
40. Mushahwar VK, Collins DF, Prochazka A. Spinal cord microstimulation generates functional limb movements in chronically implanted cats. *Exp Neurol*. 2000;163(2):422-429.
41. Bamford JA, Todd KG, Mushahwar VK. The effects of intraspinal microstimulation on spinal cord tissue in the rat. *Biomaterials*. 2010;31(21):5552-5563.
42. Biran R, Martin DC, Tresco PA. Neuronal cell loss accompanies the brain tissue response to chronically implanted silicon microelectrode arrays. *Exp Neurol*. 2005;195(1):115-126.
43. Obaid A, Wu YW, Hanna M, Nix W, Ding J, Melosh N. Ultra-sensitive measurement of brain penetration with microscale probes for brain machine interface considerations. *bioRxiv*. Preprint published online October 29, 2018. doi:10.1101/454520
44. Boergens KM, Tadić A, Hopper MS, et al. Laser ablation of the pia mater for insertion of high-density microelectrode arrays in a translational sheep model. *J Neural Eng*. 2021;18(4):045008.
45. Dobariya A, El Ahmadieh TY, Good LB, et al. Recording of pig neuronal activity in the comparative context of the awake human brain. *Sci Rep*. 2022;12(1):15503.

Disclosures

Dr. Toossi reported a patent for US11058510B2 issued. Dr. Konrad reported consulting and grants from Medtronic outside the submitted work and a patent for US #62/562,197 pending.

Author Contributions

Conception and design: Mushahwar, Hu, Everaert, Robinson, Konrad. Acquisition of data: Mushahwar, Hu, Everaert, Toossi, Kang, Tyreman, Dalrymple, Robinson, Uwiera, Shah, Fox, Konrad. Analysis and interpretation of data: Mushahwar, Mirkiani, O'Sullivan, Roszko, Faridi, Hu, Fang, Tyreman, Robinson, Fox. Drafting the article: Mirkiani, O'Sullivan, Roszko, Tyreman. Critically revising the article: Mushahwar, Mirkiani, O'Sullivan, Roszko, Everaert, Toossi, Dalrymple, Robinson, Uwiera, Shah, Fox, Konrad. Reviewed submitted version of manuscript: Mushahwar, Mirkiani, O'Sullivan, Roszko, Everaert, Toossi, Tyreman, Robinson, Uwiera, Shah, Fox, Konrad. Approved the final version of the manuscript on behalf of all authors: Mushahwar. Statistical analysis: Mirkiani, Roszko, Hu. Administrative/technical/material support: Everaert. Study supervision: Mushahwar.

Supplemental Information

Online-Only Content

Supplemental material is available with the online version of the article.

Supplemental Material. https://thejns.org/doi/suppl/10.3171/2024.2.SPINE23757.

Current Affiliations

Dr. Dalrymple: Department of Biomedical Engineering and Department of Physical Medicine and Rehabilitation, University of Utah, Salt Lake City, Utah.

Correspondence

Vivian K. Mushahwar: Neuroscience and Mental Health Institute, University of Alberta, Edmonton, AB, Canada. vivian.mushahwar@ualberta.ca.